JOURNAL PRE-PROOF

This is an early version of the article, published prior to copyediting, typesetting, and editorial correction. The manuscript has been accepted for publication and is now available online to ensure early dissemination, author visibility, and citation tracking prior to the formal issue publication.

It has not undergone final language verification, formatting, or technical editing by the journal's editorial team. Content is subject to change in the final Version of Record.

To differentiate this version, it is marked as "PRE-PROOF PUBLICATION" and should be cited with the provided DOI. A visible watermark on each page indicates its preliminary status.

The final version will appear in a regular issue of *Engineering Transactions*, with final metadata, layout, and pagination.

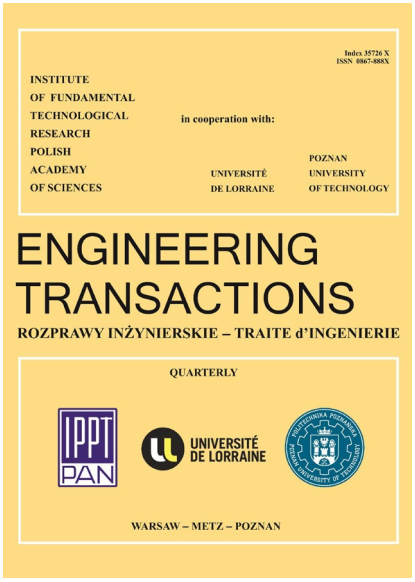

Title: Caustics Formation by a Spherical Reflector – Geometric and Wave Field Analysis with Applications in Room Acoustics and Radio Astronomy

Author(s): Andrzej Kulowski

DOI: https://doi.org/10.24423/engtrans.2026.3594

Journal: *Engineering Transactions*

ISSN: 0867-888X, e-ISSN: 2450-8071

Publication status: In press

Received: 2025-06-24

Revised: 2025-10-26

Accepted: 2026-01-29

Published pre-proof: 2026-02-02

Please cite this article as:

Kulowski A., Caustics Formation by a Spherical Reflector – Geometric and Wave Field Analysis with Applications in Room Acoustics and Radio Astronomy, *Engineering Transactions*, 2026, https://doi.org/10.24423/engtrans.2026.3594

Caustics Formation by a Spherical Reflector – Geometric and Wave Field Analysis with Applications in Room Acoustics and Radio Astronomy

Andrzej KULOWSKI
Faculty of Architecture, Gdańsk University of Technology,
Gdańsk, Poland
e-mail: kulowski@pg.edu.pl
ORCID: 0000-0001-7003-9515

This paper was presented orally at the 95th Annual Meeting of the International Association of Applied Mathematics and Mechanics GAMM2025, Poznań, April 7th-11th, 2025.

Based on the principles of geometrical optics, an analytical description of caustics generated in a spherical mirror is presented. The formation of caustics in a wave field is studied using acoustic and electromagnetic waves as an example. Symmetry of equations describing energy relations in acoustics and electromagnetism is shown. The presence of caustics in natural phenomena is demonstrated, as well as their manifestation in architectural acoustics and astronomy. It is explained why in the sound field in existing halls, rather than the entire caustics, only their cusp is observed, which is perceived as a blurred area with an increased sound level accompanied by unusual values of acoustic room parameters. The influence of caustics on the efficiency of spherical and parabolic antennas used in radio astronomy is discussed.

Keywords: heritage of science, Leonardo da Vinci, caustic, spherical reflector, parabolic reflector, room acoustics, Arecibo, FAST.

1. INTRODUCTION

This article has been inspired by caustic sketches from Leonardo da Vinci's notebooks. In these drawings he uses the law of reflection, published in its full form about 100 years later by the Dutch astronomer and mathematician Willebrord Snell. Leonardo noticed that the rays reflected from a spherical mirror overlap, eventually create a focus (Fig. 1a). However, the initial stage of rays' concentration known today as caustics was not the subject of his interest. Leonardo's drawings clearly present the mechanism of caustics, but he did not elaborate on this topic, apparently not realizing the importance of his discovery.

Leonardo's drawings show that he was aware of the difference between spherical and parabolic concave mirrors. With an infinitely distant source of rays a spherical mirror will always create a focus accompanied by caustics, while a parabolic mirror creates a focus without caustics (Fig. 1). Leonardo thus had a ready-made device that effectively fulfilled his postulate of concentrating all the rays at one point, i.e., a parabolic mirror. However, he did not use it and continued his research using a spherical mirror. He was interested in the utility of a mirror as a device to heat or even boil water, which was an ambitious technical idea in his time (Fig. 2).

Concentration of light in the form of caustics is a common side effect of natural or artificial lighting. It accompanies numerous situations in everyday life and is also an element of natural phenomena. Two types of caustics can be distinguished here, namely catacaustics produced by

reflection of light, and diacaustics, produced by refraction of light at the boundary of media, e.g., air and water (Fig. 3, 4). This article examines the conditions under which catacaustics are formed.

The aim of this article is to examine the extent to which the caustics phenomenon discovered by Leonardo is present in contemporary research and technology.

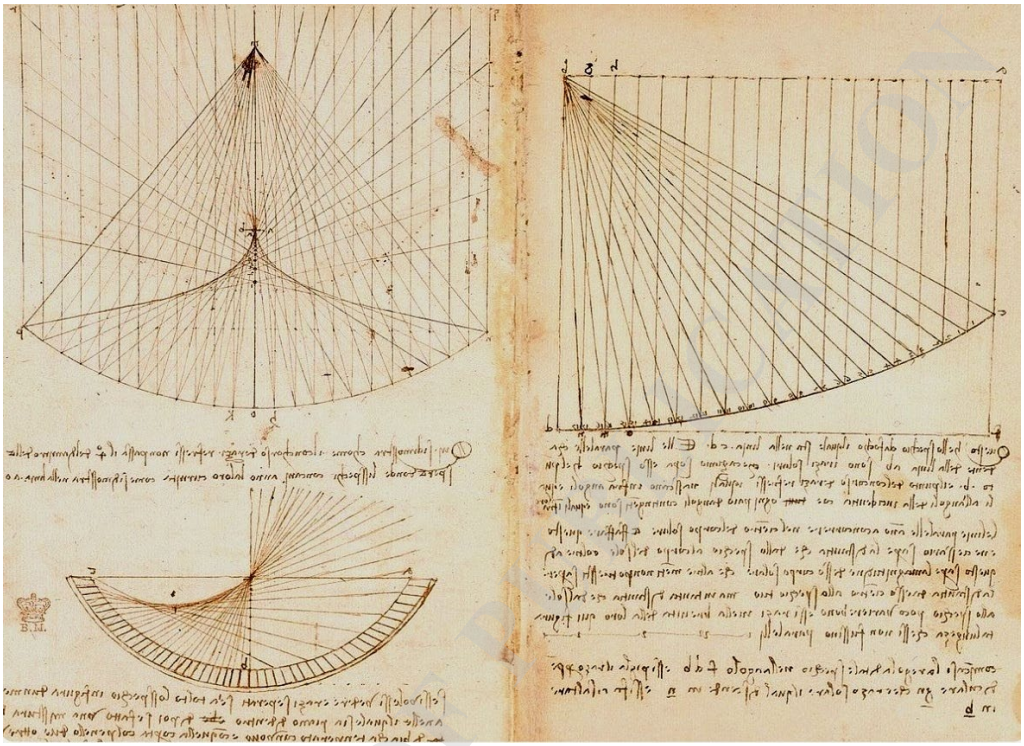

a) b)

Fig. 1. Leonardo da Vinci's studies on the reflection of light by a spherical (a) and parabolic mirror (b) [1]

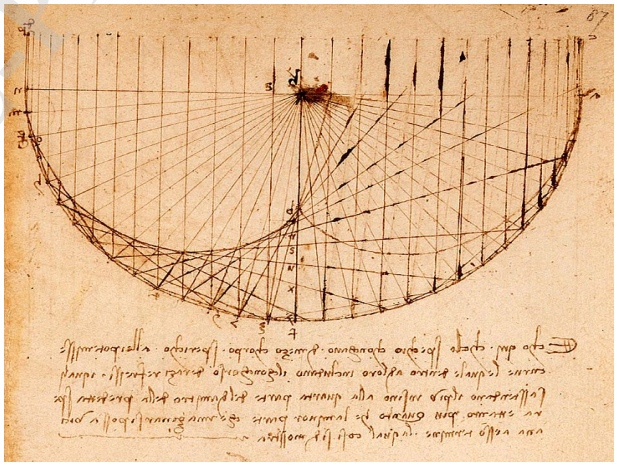

Fig. 2. The most advanced drawing of a caustic from Leonardo's notes [2]. *According to the commentary written in his famous reverse handwriting, "In concave mirrors of the same diameter, the one that has the shallower curvature will concentrate the greatest number of reflected rays at the focal point, and consequently will kindle a fire with greater rapidity and force".*

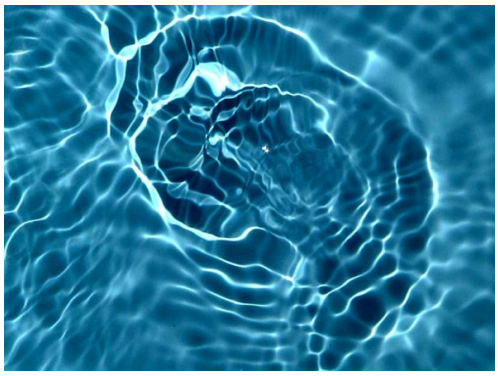

(a) Photo courtesy of J.L. Jankowski [13]

(b)

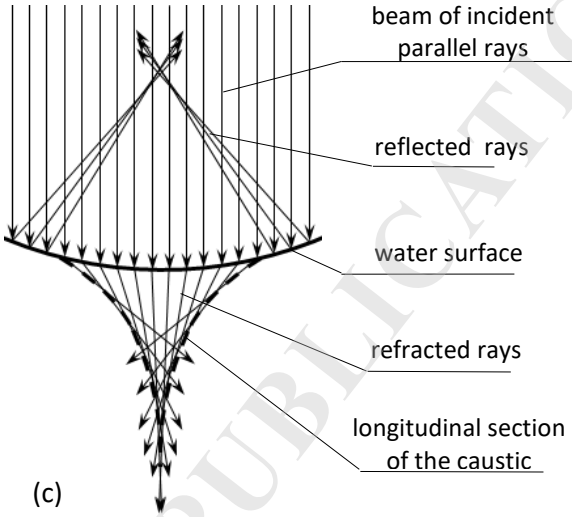

(c)

Fig. 3. Diacaustics (a) and cataustics (b) produced by refraction and reflection of sunlight. The course of rays (c) leading to the formation of cataustics below and diacaustics above the water surface [4], [9].

The rainbow [5]

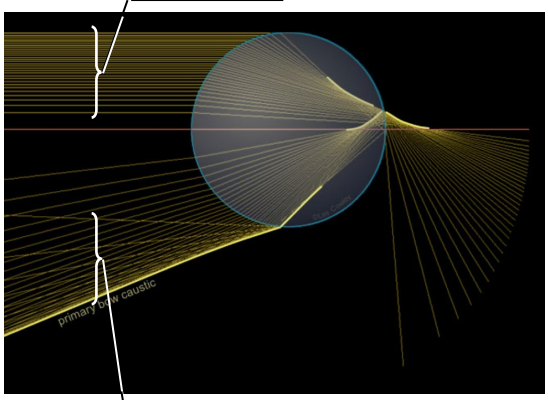

The light split on a drop of water into primary colors, creating a rainbow phenomenon. Cata-caustics inside and diacaustics outside the drop are shown [6].

Fig. 4. The formation of a rainbow is accompanied by caustics twice: inside the water droplet the catacaustic is formed, while outside the diacaustic is formed

2. SOURCE AT INFINITE DISTANCE FROM THE SPHERICAL MIRROR

2.1. ANALYTICAL DESCRIPTION OF THE CAUSTIC

The literature provides numerous examples of graphical constructions and computer simulations of caustics formation in concave mirrors of various shapes [7], [8]. These works represent a contemporary continuation of Leonardo's graphical approach to caustics. This chapter presents an analytical description of the caustics generated by a spherical mirror when the source of rays is at an infinite distance.

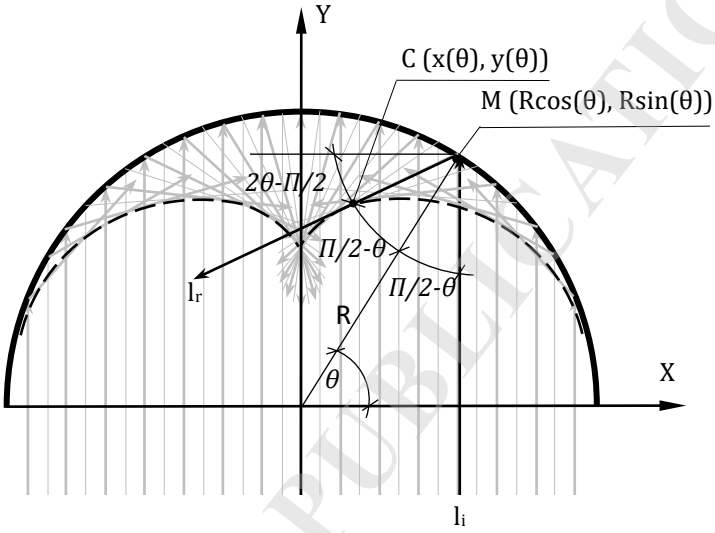

Fig. 5. Reflection of the ray by a concave spherical or hemi-cylindrical mirror with an infinitely distant source of rays. l_i, l_r: the incident and reflected ray; M: the reflection point; C: the point on the caustic; R: the radius of the sphere [9]

The derivation of the caustic equation involves (Fig. 5) [9]:

- creating Eq. (2.1) of a straight line l_r showing the direction of the reflected ray. Line l_r is an element of caustics.

$$y(x,\theta) = -\frac{\mathrm{x}}{\mathrm{tg}(2\theta)} + R\left(\sin(\theta) + \frac{\cos(\theta)}{\mathrm{tg}(2\theta)}\right) \tag{2.1}$$

- creating Eq. (2.2) showing infinitesimal small changes in the slope of the line l_r

$$\mathrm{d}y(x,\theta)/\mathrm{d}\theta = 0 \tag{2.2}$$

- solving Eq. (2.2) and presenting the solution in the form (2.3)

$$\begin{cases} \mathrm{x}(\theta) = \mathrm{R}\cos^3(\theta) \\ y(\theta) = \dfrac{\mathrm{R}}{2}\left(2\sin^3(\theta) - 3\sin(\theta)\right) \end{cases} \qquad 0 \le \theta \le \Pi \tag{2.3}$$

2.2. SURFACE DENSITY OF THE RAYS ENERGY ON THE CAUSTIC

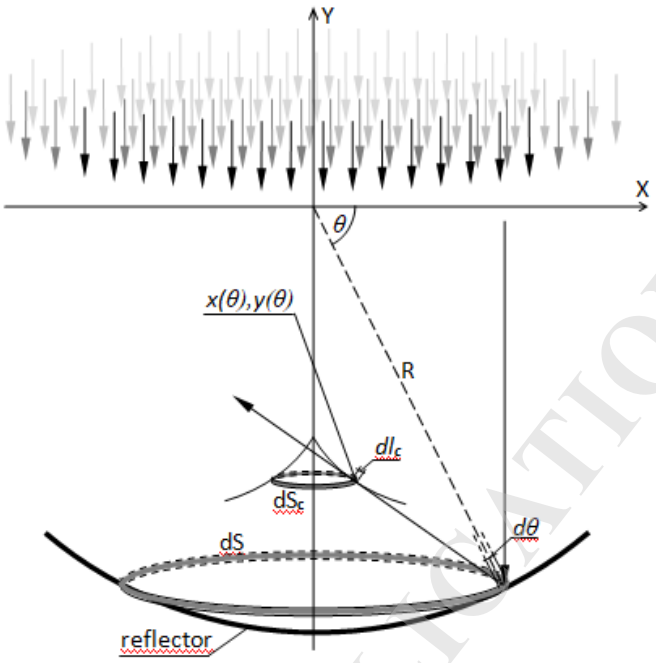

Fig. 6. The caustic formed by rays incident on a hemispherical reflector. R: radius of the reflector, dS, dS_c: the ring on the reflector and on the caustic, x(θ),y(θ): Cartesian coordinates of the caustic (Eq. (2.3)), dl_c: the element of the section of the caustic [10], [12]

Consider two rings inside a bowl: dS on its surface and dS_c on a caustic (Fig. 6). The rays reflected from the ring dS are tangent to the ring dS_c. This means that the energy on dS is the same as the energy on dS_c. Areas dS, dS_c of the rings are [13]

$$dS = 2\Pi R^2 \cos(\theta) \sin(\theta)\, d\theta \tag{2.4}$$

$$dS_c = 3\Pi R^2 \cos^4(\theta)\, d\theta \tag{2.5}$$

so the surface density of rays' energy on the caustics per unit time, i.e., the surface power density of rays, is equal to the ratio of the areas of the rings.

$$C(\theta) = \frac{dS}{dS_c} = \frac{2\sin(\theta)}{3\,|\cos^3(\theta)|} \tag{2.6}$$

As for axial incidence of rays the area dS_c tends to zero, Eq. (2.6) creates a singularity for θ=0,5 rad, which corresponds to the caustic's cusp.

The total ray intensity over the caustic $I_{c,res}(\theta)$ consists of the energy of incident rays I_o and the energy of the reflected rays concentrated on the caustic

$$I_{c,res}(\theta) = \mathrm{I_o} + \mathrm{I_o}(1-\alpha)\frac{2\sin(\theta)}{3\,|\cos^3(\theta)|} = \mathrm{I_o}\left(1 + (1-\alpha)\frac{2\sin(\theta)}{3\,|\cos^3(\theta)|}\right) \quad [\mathrm{W/m^2}] \tag{2.7}$$

The derivation of equations (2.4)-(2.7) is presented in the bibliography [10]. The ray intensity level on the caustic, with I_o as the reference intensity, is given by the equation (2.8) (see Fig. 7):

$$L_{c,res}(\theta) = 10\log\frac{I_{c,res}(\theta)}{I_o} = 10\log\left(1+(1-\alpha)\frac{2\sin(\theta)}{3\,|\cos^3(\theta)|}\right) \quad \text{[dB]} \qquad (2.8)$$

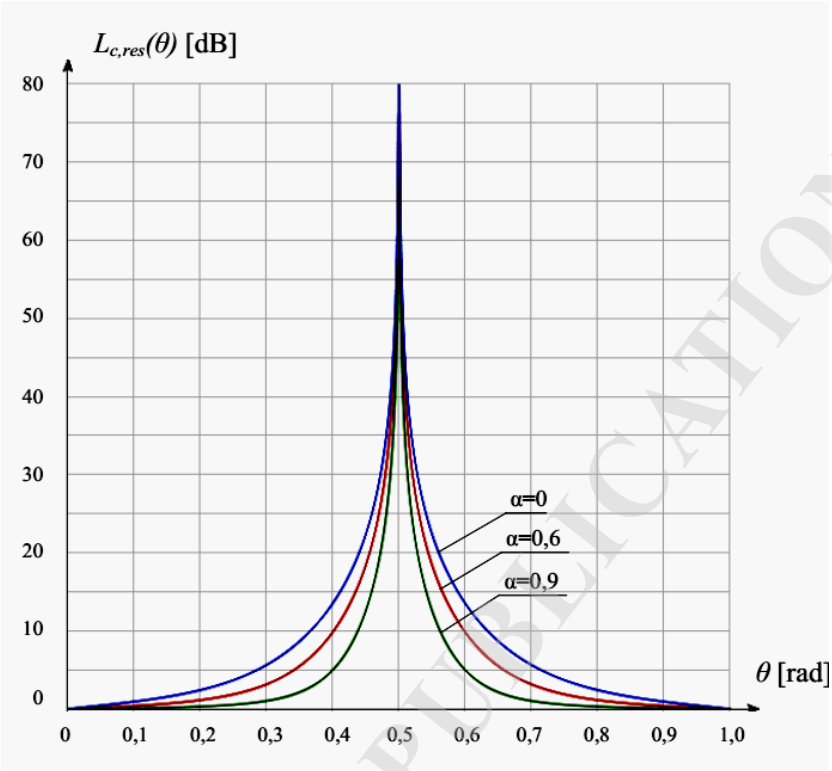

Fig. 7. Rays intensity level $L_{c,res}(\theta)$ [dB] on the caustic (graph of Eq. (2.8))
α: absorption coefficient of the reflector [10]

3. SOURCE AT FINITE DISTANCE FROM THE SPHERICAL MIRROR

If the source of rays S is located at a finite distance d from the mirror, the derivation of the caustic equation is similar to that in Section 2.1, but using different relations [10]:

- Constructing the equation $y(x,\varphi\text{-}\theta)$ of the line ℓ_r (Fig. 8) and expressing it as a function of θ (Eq.(3.1),
- Deriving the analytical form of $dy(x,\theta)/d\theta$, and then solving the equation $dy(x,\theta)/d\theta = 0$ (Eq.(3.3)) and presenting the solution in the form $y=f(x,\theta)$ (Eq.(3.4)-(3.6)):

$$y(x,\theta) = \text{tg}(\varphi\text{-}\theta)(x\text{-}R\cos(\theta)) - R\sin(\theta) \qquad (3.1)$$

where

$$\varphi(\theta) = \arcsin\left(\frac{d\cos(\theta)}{\sqrt{R^2+d^2+2Rd\sin(\theta)}}\right) \qquad (3.2)$$

$$\frac{dy}{d\varphi} = \frac{x - R\cos(\theta)}{\cos^2(\varphi-\theta)}\left(2+\frac{R\cos(\varphi)}{\sqrt{d^2-R^2\sin^2(\varphi)}}\right) - R\left(\text{tg}(\varphi-\theta)\sin(\theta)-\cos(\theta)\right)\left(1+\frac{R\cos(\varphi)}{\sqrt{d^2-R^2\sin^2(\varphi)}}\right) = 0 \qquad (3.3)$$

$$\begin{cases} x(\theta) = R\left(-\cos(\theta) + \sin(\theta)\times tg\left(\Gamma(\theta)\right)\right)\times \cos^2\left(\Gamma(\theta)\right)\times \dfrac{R^2 + d^2 + 2Rd\sin(\theta)}{R^2 + 2d^2 + 3Rd\sin(\theta)} + R\cos(\theta) & (3.4) \\ y(x,\theta) = \left(x(\theta) - R\cos(\theta)\right)tg\left(\Gamma(\theta)\right) - R\sin(\theta) & (3.5) \end{cases}$$

where

$$\Gamma(\theta) = \arcsin\left(\frac{d\cos(\theta)}{\sqrt{R^2 + d^2 + 2Rd\sin(\theta)}}\right) - \theta\,, \qquad 0 \le \theta \le \Pi. \qquad (3.6)$$

The detailed derivation Eq. (3.4)-(3.6) is presented in the bibliography [13]. The graph of the set of equations (3.4) and (3.5) is shown in Fig. 9. For $d \to \infty$ these equations reduce to the form (2.3) which corresponds to the case of an infinitely distant source of rays (see Appendix).

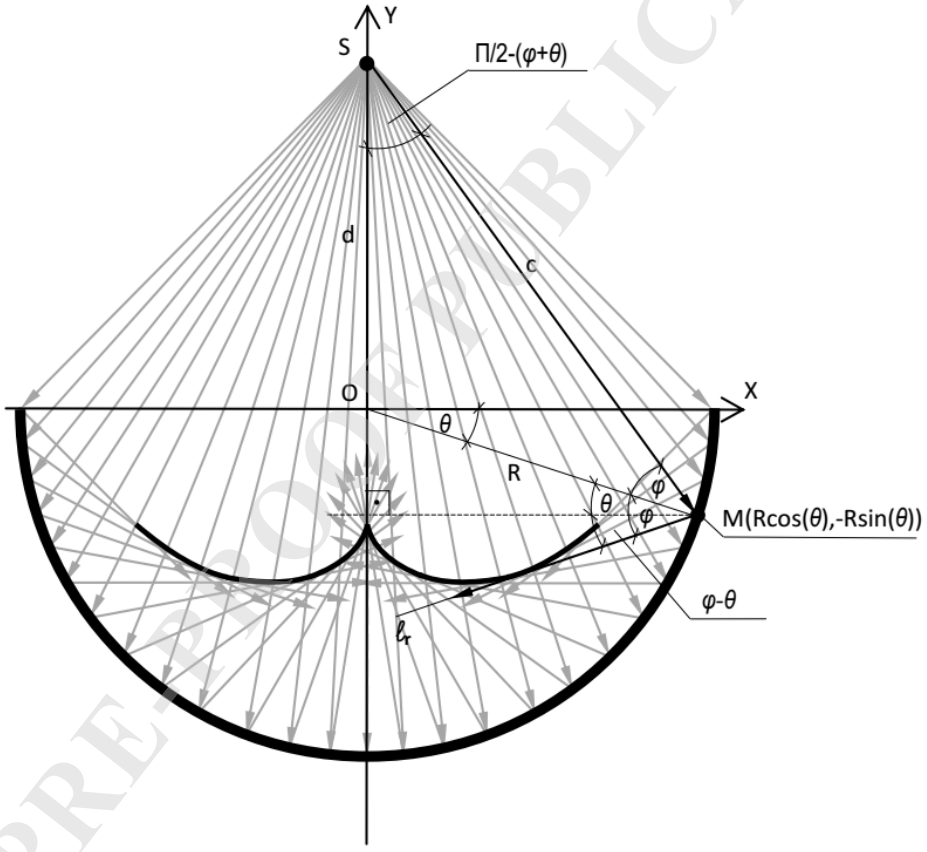

Fig. 8. Reflection of the ray by a concave spherical or hemi-cylindrical mirror with a given distance between the mirror and the source of rays. S: the source of rays, R: the mirror radius, ℓ_r: the straight line describing the reflected ray [10]

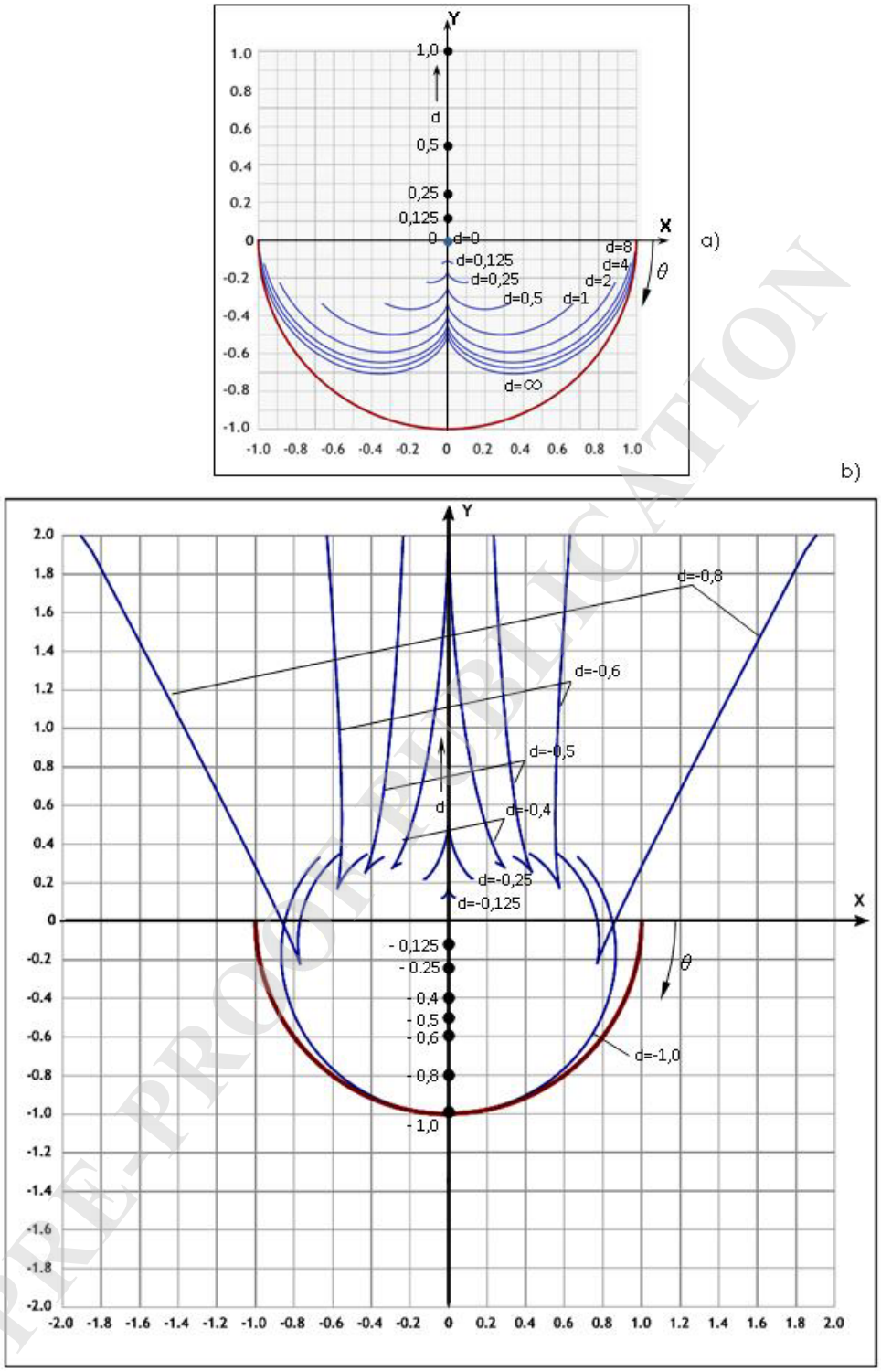

Fig. 9. Graph of the set of Eq. (3.4) and (3.5) for the source of rays outside (d positive) and inside the bowl (d negative) [10]

4. CAUSTICS IN A WAVE FIELD

As the incident wave propagates through the reflector dish, it interferes with the reflected wave, producing a series of interference fringes that fill the dish itself and the space in front of it. The wave nature of the field also causes deflection at the mirror's edge [10], [11]. This chapter describes the effect occurring only on a caustic itself, i.e., the interference of incident and reflected waves on the hypersurface forming the caustic; therefore the above-mentioned edge effects are omitted.

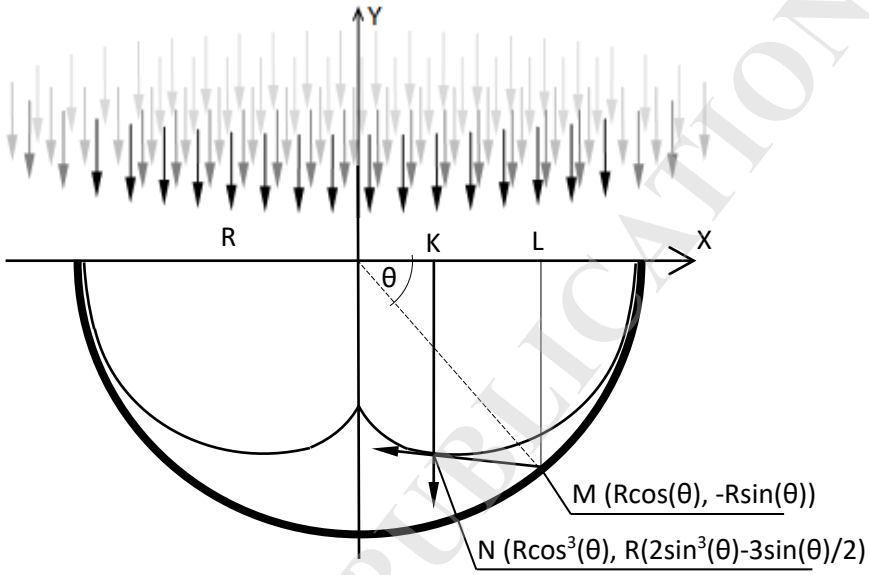

Fig. 10. The scalar superposition of incident and reflected waves KN and LMN on the caustic. R: radius of the reflector [10]

Assume that all incoming rays reach the plane y=0 at the same time. They can therefore be treated as the front of a plane wave, e.g., an acoustic wave (Fig. 10). The sound pressure in the y=0 plane is then $p_i(\mathrm{t}) = \sqrt{\mathrm{I_o}\rho\mathrm{c}}\,\sin\varpi t$, where w=2Πf, f: frequency [Hz]. The sound pressure of the incident and reflected waves at point N of the caustics are p_{KN}(t) and p_{LMN}(t) (Eq. (4.1), (4.2)). These are scalar values, so their sum is $\mathrm{p_{c,res}}$(t) (Eq. (4.3)):

$$p_{KN}(\mathrm{t}) = \sqrt{\mathrm{I_o}\rho\mathrm{c}}\,\sin\varpi\left(t+\Delta t_1\right) \qquad \Delta \mathrm{t}_1 = \frac{\mathrm{R}}{2}\left(3\sin(\theta)-2\sin^3(\theta)\right)/\mathrm{c} \qquad (4.1)$$

$$p_{LMN}(\mathrm{t}) = \sqrt{\mathrm{I_o}\rho\mathrm{c}}\,\sqrt{\frac{2(1-\alpha)\sin(\theta)}{3\,|\cos^3(\theta)|}}\,\sin\varpi(\mathrm{t}+\Delta \mathrm{t}_2) \qquad \Delta \mathrm{t}_2 = \frac{\mathrm{R}}{2}3\sin(\theta) \qquad (4.2)$$

$$p_{c,res}(\mathrm{t}) = \sqrt{\mathrm{I_o}\rho\mathrm{c}}\left(\sin\varpi(\mathrm{t}+\Delta \mathrm{t1}) + \sqrt{\frac{2(1-\alpha)\sin(\theta)}{3\,|\cos^3(\theta)|}}\,\sin\varpi(\mathrm{t}+\Delta \mathrm{t}_2)\right) \quad [\mathrm{Pa}] \qquad (4.3)$$

The sound pressure amplitude $p_{c,res}$(t) varies along the caustics. Fluctuations take the form of amplitude modulation and the condition of reaching the extreme is $\frac{\mathrm{d}}{\mathrm{dt}}\,p_{c,res}(\mathrm{t}) = 0$. The solution of this equation is $p_{c,res,Max}(\theta)$, which describes maxima and minima of the fluctuations along the caustics [10], [13] (Eq. (4.4), Fig. 11):

$$p_{c,res,Max}(\theta) = \sqrt{\frac{I_o}{2\rho c}}\left[\sin\left(\text{arctg}\left(q\right)\right) + \sqrt{\frac{2(1-\alpha)\sin(\theta)}{3\,|\cos^3(\theta)|}}\sin\left(\text{arctg}\left(q\right) + \varpi\frac{R\sin^3(\theta)}{c}\right)\right] \quad \text{[Pa]} \quad (4.4)$$

$$q = \frac{\sqrt{\frac{3\,|\cos^3(\theta)|}{2(1-\alpha)\sin(\theta)}} + \cos\left(\varpi\frac{R\sin^3(\theta)}{c}\right)}{\sin\left(\varpi\frac{R\sin^3(\theta)}{c}\right)}$$

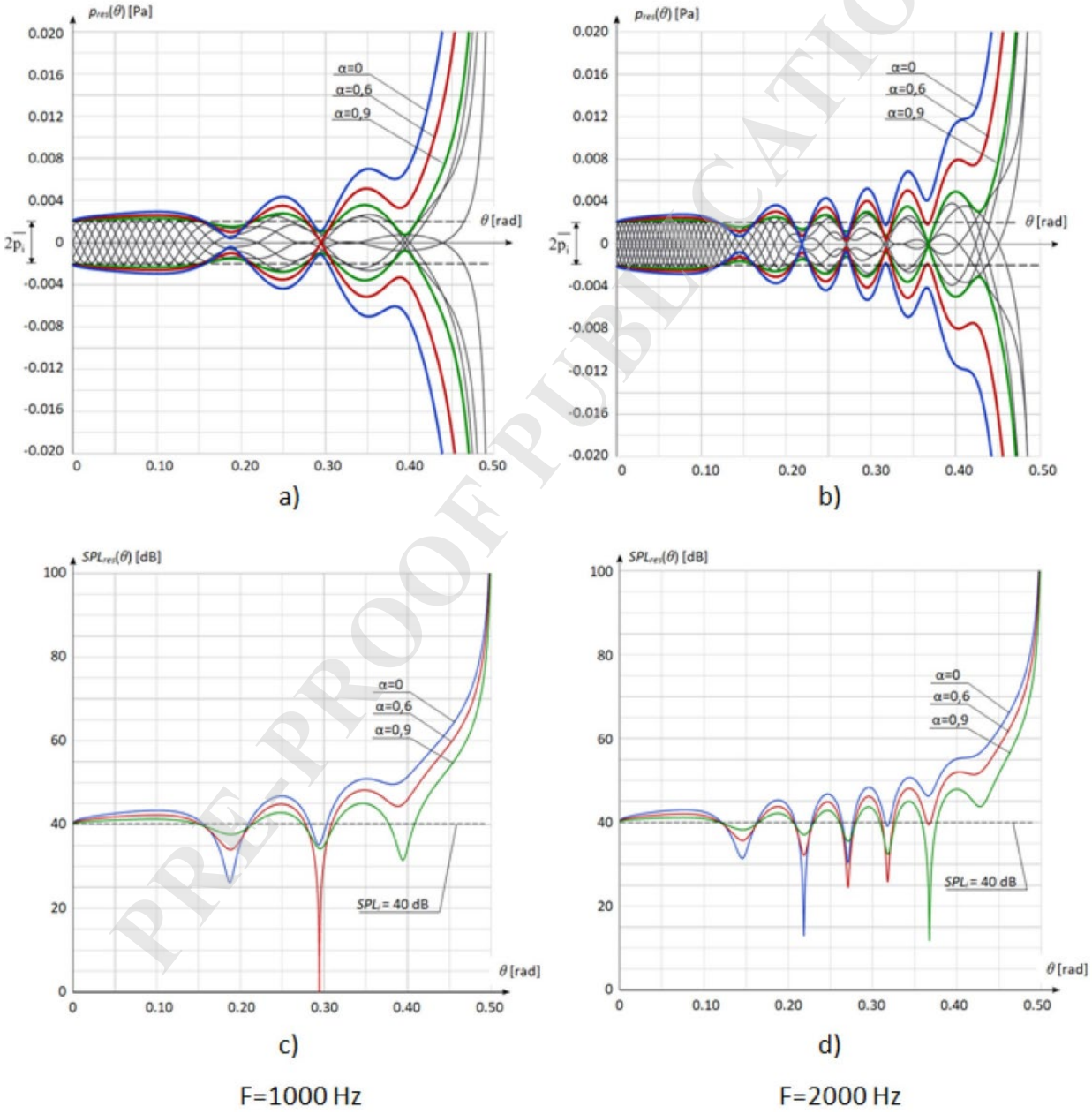

Fig. 11. Graph of Eq. (4.4). Black: instantenous state of fluctuation shown every 1/8 of period; blue, red and green: extremes of the fluctuations with no absorption, 60% absorption, and 90% absorption during reflection, respectively

The conclusions from Eq. (4.4) are as follows:

- The fluctuation takes the form of local increases and decreases in the sound pressure amplitude along the caustics. This may explain why caustics are difficult to observe under real indoor conditions, especially in the presence of reflections and background noise.
- The fluctuations disappear as the caustics approach the focus. This is because the difference between the paths of the incident and reflected waves then approaches zero. This means that there are no fluctuations at the focus. Consequently, the focus is easier to detect then the caustics themselves.

Despite the different nature of acoustic and electromagnetic waves, a pair of physical quantities, which are the sound intensity I_s and the surface power density of electromagnetic field I_e, are described by the same equation, but with different interpretations of individual components (Eq. (4.5), (4.6)), [13]. The same applies to the sound pressure $\overline{p_c(\theta)}$ and the electric field's intensity $\overline{E_c(\theta)}$ condensed on the caustic (Eq. (4.7), (4.8)):

$$I_s = p^2/(\rho c_s) \quad [W/m^2] \qquad I_e = E^2/(\mu_o c_l) \quad [W/m^2] \tag{4.5), (4,6}$$

$$\overline{p_c(\theta)} = \sqrt{I_{c,s}(\theta)\rho c_s} = \sqrt{I_o \rho c_s}\sqrt{\frac{2(1-\alpha)\sin(\theta)}{3|\cos^3(\theta)|}} \quad [Pa] \qquad \alpha = \frac{I_{abs}}{I_i} = \left(\frac{\overline{p_{abs}}}{\overline{p_i}}\right)^2 \tag{4.7}$$

$$\overline{E_c(\theta)} = \sqrt{I_{c,em}(\theta)\mu_0 c_\ell} = \sqrt{I_{em}\mu_0 c_\ell}\sqrt{\frac{2R\sin(\theta)}{3|\cos^3(\theta)|}} \quad [V/m] \qquad \mathcal{R} = \left(\frac{\overline{E_{refl}}}{\overline{E_i}}\right)^2 \tag{4.8}$$

where

p: sound pressure [Pa],

E: intensity of the electric field [V/m],

c_s, c_l: speed of sound in the air and speed of light, c_s = 331 m/s, $c_l = 3*10^8$ [m/s],

ρ: density of the medium, in the air ρc_s = 415[kg/(m^{2}s),

μ_o: vacuum permeability, $\mu_o = 4\Pi 10^{-7}$, [H/m],

$I_{c,s}(\theta)$: sound intensity on the caustic, [W/m^2],

$I_{c,em}(\theta)$: surface power density of the electromagnetic field on the caustic, [W/m^2],

I_o: intensity of the incident sound, [W/m^2],

I_{em}: surface power density of the electromagnetic field, of the incident wave, [W/m^2].

α: sound absorption coefficient,

R : reflection coefficient of the electric component of the electromagnetic wave.

An electromagnetic wave is a vector wave, and the result of the superposition of the incident and reflected waves is their vector sum (Fig. 12). Equation (4.4) relates to scalar field and has no equivalent for the vector nature of the electromagnetic field. However, when an incoherent electromagnetic wave is considered, e.g., the one that reaches the dish of the radio telescope from deep space, the phenomenon in question is consistent with geometric optics. This allows for scalar summation of the electric field intensities of the incident and reflected waves, analogous to the scalar summation of acoustic pressures.

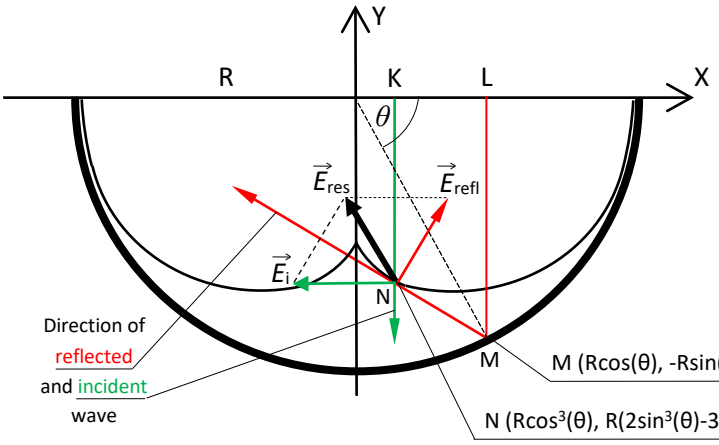

Fig. 12. Vector superposition of electric components E_i and E_{refl} of incident and reflected electromagnetic waves KN and LMN on the caustic. It has been assumed that the waves are linearly polarized and the plane of polarization lies in the plane of the drawing. R: radius of the reflector

5. CAUSTICS IN ROOM ACOUSTICS

The typical response of rooms to speech and music is a sequence of sound built-up and decay. As a result, when a sound concentration effect in the form of caustics appears in a room, it is less noticeable than when excited by a continuous sound signal. Moreover, the high dynamics and wide spectrum of sound signals that constitute speech and music, combined with wave phenomena, reverberation and background noise make it difficult to identify caustics aurally. The image of caustics may also be blurry due to the sound pressure fluctuations on the caustics (Fig. 11). Therefore, at high intensities of these masking agents, only the cusp of the caustics is audible, manifesting as a point-like concentration of sound, while the rest of the caustics seems to be absent.

Furthermore, in a typical auditorium situation, listeners do not move and therefore do not experience areas of higher and lower sound levels. It can therefore be expected that in halls with the audience sitting in theatre seats, the auditory symptoms of acoustic foci are mainly distortions in the perception of sound timbre, deformation of directional effects, reduced speech intelligibility, etc. [14].

An example of a room where caustics are formed is the Poznań University auditorium (Fig. 13). This hall is known for its good acoustics, and hosts International violin competitions, which have a great reputation in the world of music. The concave ceiling of the hall creates a caustic, but the sound focusing area is high above the audience and does not affect the acoustics of the hall.

In the Lviv Opera Hall, caustics are present in the audience area. At the sound source on the stage, the sound concentration covers the niche created by the balcony in the rear part of the audience. To prevent possible adverse effects, the rear wall was covered with diffusers that disperse the sound reflected off the rear wall (Fig. 14). Acoustic measurements have shown that the sound concentration effect occurs in the audience, but is barely perceptible to hearing (Fig. 15).

In large public spaces with geometry that promotes the formation of caustics, the phenomenon of sound concentration along with the above-mentioned accompanying effects may be completely unnoticeable due to the afore-said disturbances, high level of background noise, as well as the presence of numerous sound sources, typical in such places (Fig. 16, 17).

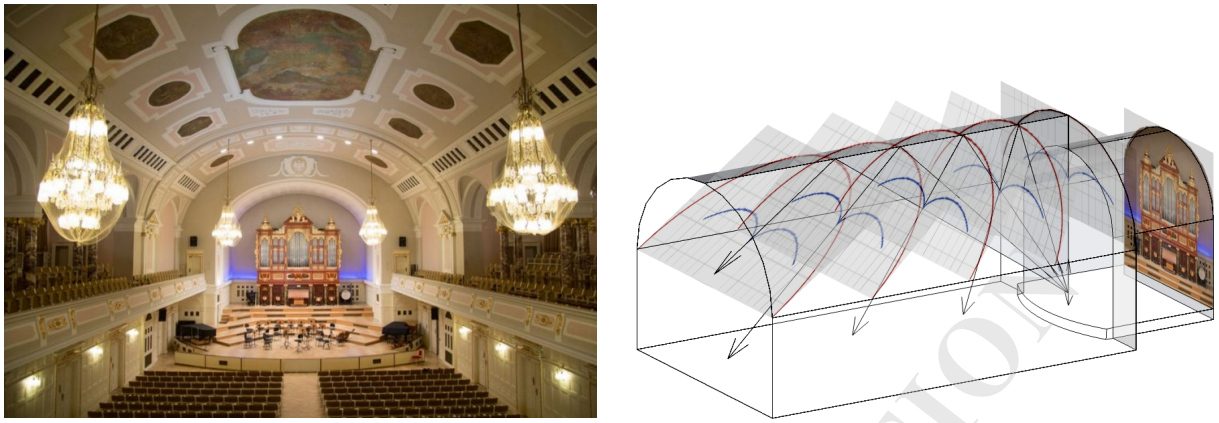

a) b)

Fig. 13. a) Poznań University auditorium with an arched vault typical of auditoriums of that period. This Neo-Renaissance building was erected according to the design of Edward Fürstenau in 1905-1910. Photo courtesy of Poznań Film Commission [15]. *b) The caustic formed by the concave ceiling of the hall* [10]

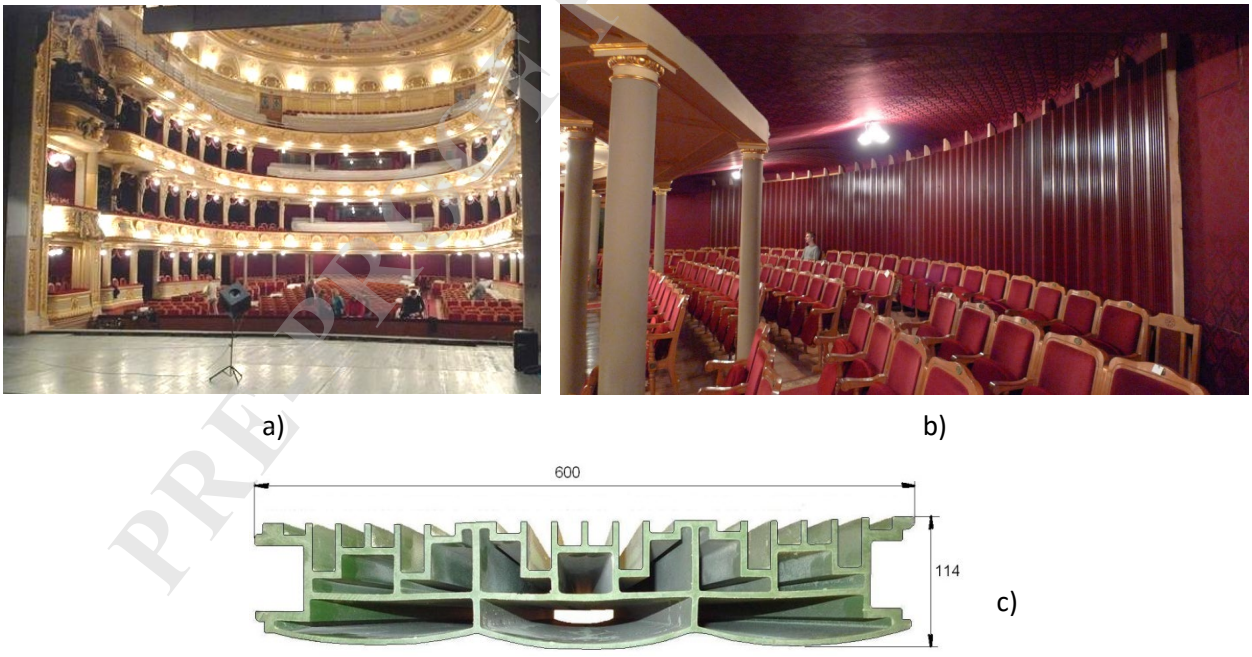

a) b) c)

Fig. 14. Neo-Renaissance hall of the Lviv Opera designed by Zygmunt Gorgolewski (1897-1900) (a) with a back wall on a circular plan (b). To prevent adverse phenomena created by caustics in the rear part of the audience area, the rear wall was covered with diffusers (c) [16]

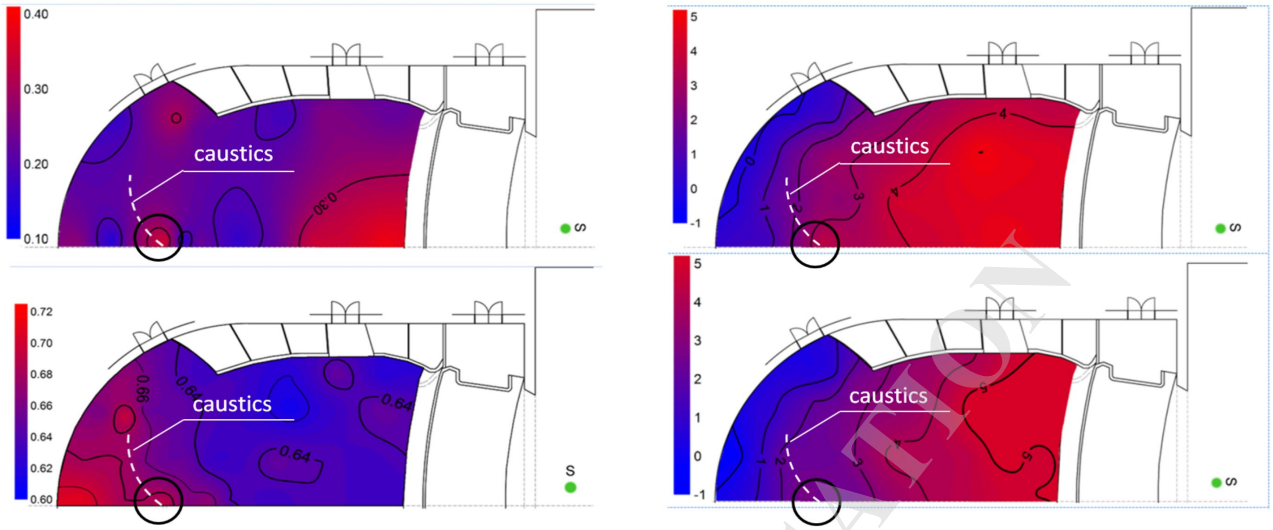

Fig. 15. Measurement results of caustics created in the audience in Lviv Opera Hall. Black circle: the cusp of caustics. a) Distribution of the measured parameter in the audience: top - Interaural Cross Correlation $IACC_{500\text{-}1000}$, bottom: Speech Transmission Index STI. b) Sound Strength $G_{4000\ Hz}$ before (top) and after (bottom) the sound diffusers were installed. The use of diffusers limited the value of $G_{4000\ Hz}$ by 2 dB. In all the cases the sound concentration effect in a form of caustic is measurable but barely perceptible to hearing [17]

Fig. 16. The market hall in Gdynia with a parabolic roof, built in 1938 in the constructivist style. Photo by A. Kulowski

Fig. 17. Market Hall in Rotterdam, Netherlands, under 40-metre-tall arch, built in 2014. Photo by A. Kulowski

When the acoustic mirror operates outdoors, the structure of the sound field is close to a free field. The effect of sound concentration is then much more pronounced than in the room and can be used for practical purposes, for example for demonstration or for listening to distant noise sources (Fig. 18). The resulting acoustic effect shows how much the acoustic disturbances in a room change the nature of the same phenomena observed in their interference-free form.

a) b)

Fig. 18. a) Grottoes of Whispers in Oliwa Park in Gdańsk (2nd half of the 18th century). Each cave is 1/4 of a sphere with a radius of 1,50 m [9], [18]. *b) Outdoor installation for demonstration of transmission of sound over a distance* [19]

7. CAUSTICS IN ASTRONOMY

The radio telescope in Arecibo, Puerto Rico, was built in a natural karst crater in 1963. Its antenna is a spherical dish with a diameter of 305 m and depth of 48.3 m, the movable main platform weighs 900 tons (Fig. 19a). Initially the aperture of the reflector was small, but it was significantly upgraded in 1997 by the use of the Gregorian subreflector system, which concentrates the energy of the caustic sections adjacent to the cusp into a single focal point (Fig. 19b, 20).

Compared to the reflector analyzed by Leonardo da Vinci with an aperture contained in an opening angle of ca. 10^0, after this upgrade the relative aperture of the Arecibo radio telescope reflector is ca. 17 times larger, i.e., by an order of magnitude [13].

On December 1, 2020, the Arecibo radio telescope was destroyed by a 900-ton main platform falling onto the radio telescope's canopy.

a) b)

Fig. 19. (a) The spherical antenna of the radio telescope in Arecibo, Puerto Rico [20] *(b) Reflectors of the Arecibo Gregorian Optics* [21]

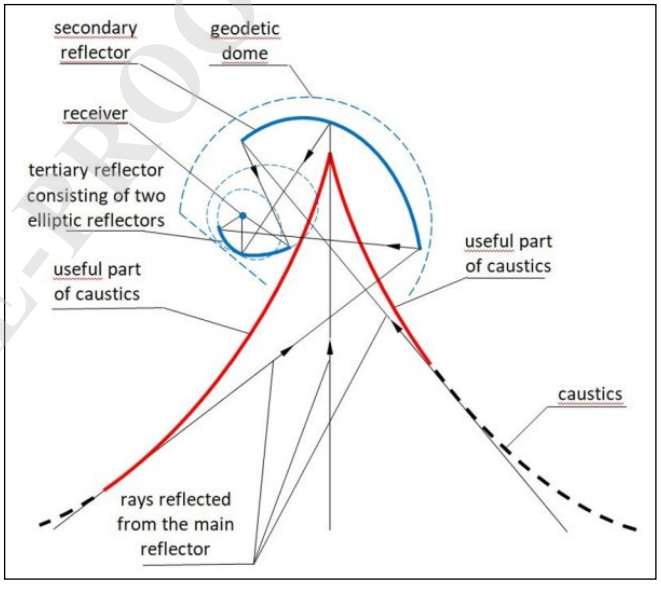

Fig. 20. Ray tracing of the secondary and tertiary reflectors of the Arecibo Gregorian Optics [13]. In addition to the energy focused on the caustic cusp, the Gregorian subreflector system also uses the energy concentrated on the part of the caustic marked red.

In 2016, 53 years after the Arecibo radio telescope was launched, another large radio telescope with a spherical antenna was built in China, also in a natural karst crater (FAST: Five-hundred-meter Aperture Spherical radio Telescope, Fig. 21a). Its dish diameter is 520 meters, which allows it to work with sphere segments with a radius of 300 meters, the same as the entire Arecibo antenna.

As in any spherical mirror, caustics are also created here, containing part of the energy reflected from the bowl. The task of recovering part of this energy was solved differently than in Arecibo. The antenna of the Chinese radio telescope consists of movable elements, the position of which can be corrected in such a way that the spherical segment of the reflector is transformed into a segment of a paraboloid (Fig. 21 b). After this upgrade, the relative aperture of the FAST reflector increased to a similar extent to that of the Arecibo radio telescope after the implementation of the Gregorian subreflector system [13].

The FAST radio telescope shows a different direction of upgrading Leonardo da Vinci's concept of ray focusing than in the Arecibo telescope. It consists of manipulating the curvature of the reflector, while in Arecibo the useful range of the caustics was manipulated.

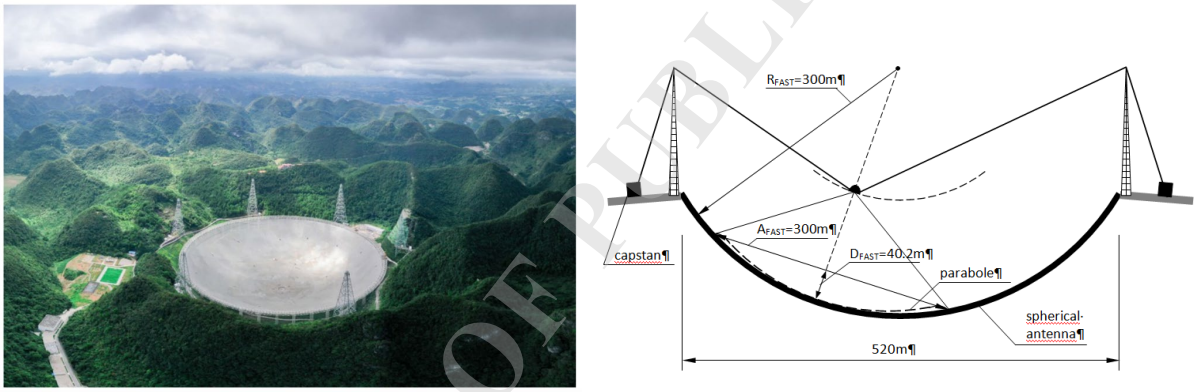

a) b)

Fig. 21. (a) Antenna of the FAST telescope (Five-hundred-meter Aperture Spherical radio Telescope) in Dawodang, China [22].
(b) Diagram of the FAST telescope. The receiver weight: 3 tons [13]

NASA (National Aeronautics and Space Administration) is considering a concept to build a 1,000-meter radio telescope in an impact crater on the far side of the Moon [23]. This is facilitated by the synchronization of the rotation of the Earth and the Moon, so that the far side of the Moon always faces away from the Earth's electromagnetic smog and the satellites orbiting the Earth. The number of craters of suitable size is 82,000, of which 50 candidates shown in Fig. 23 a) are marked with blue dots, while the crater selected for the NASA's concept is marked red [24]. The Internet even reports a concept of a radio telescope with a 25-kilometer spherical antenna [25]. However, this is a task for an army of autonomous robots, which might be implemented in the indefinite future [24]. In the longer term, consideration is being given to combining multiple radio telescopes into an interferometer with observational capabilities exceeding those of similar installations on the Earth.

The NASA concept assumes the use of a parabolic wire-mesh antenna with a fixed receiver at the focus of the parabola. Simple calculations show that due to the rotation of the Moon (with one rotation taking 27.3 days), an object contained in an angle of ±1° around the axis of the parabola can

be observed for 3h 36 min. When this object is seen from the Earth, the observation time is 9 minutes. Extending the observation angle to 2x21°=42°, as in the Arecibo spherical antenna with movable receiver (see Fig. 19 b, 20), increases this time to 76h 26 min or 2h 48 min for an observer on the far side of the Moon and on the Earth, respectively (Fig. 22).

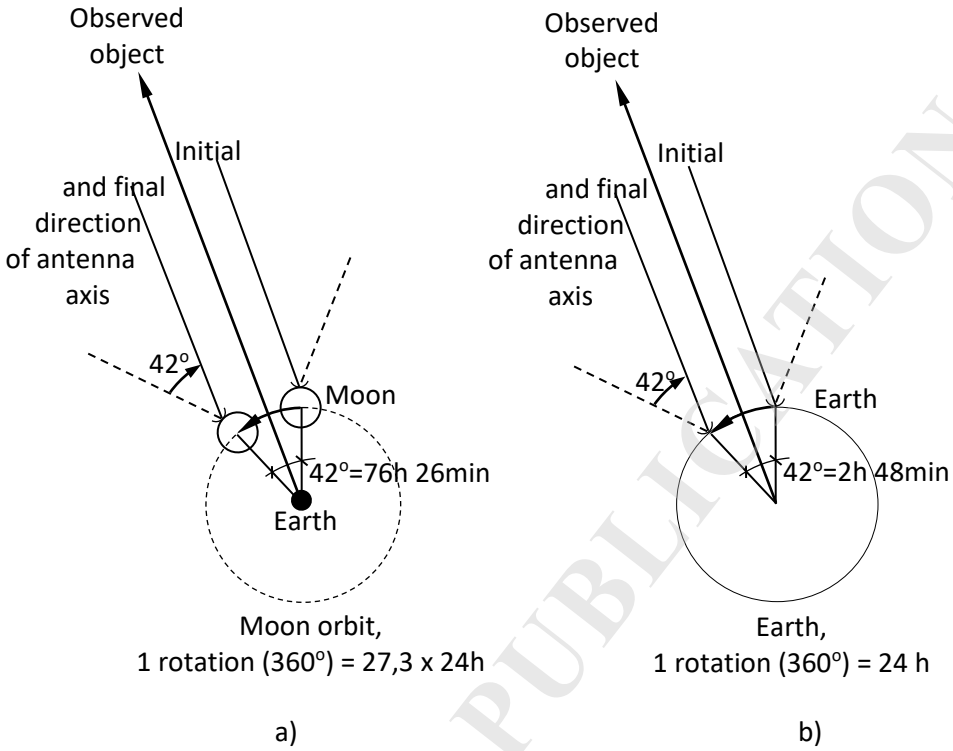

Fig. 22. Estimation of the observation time using a spherical antenna with movable receiver. An observer on the far side of the Moon (a) and on the Earth (b). Not to scale.

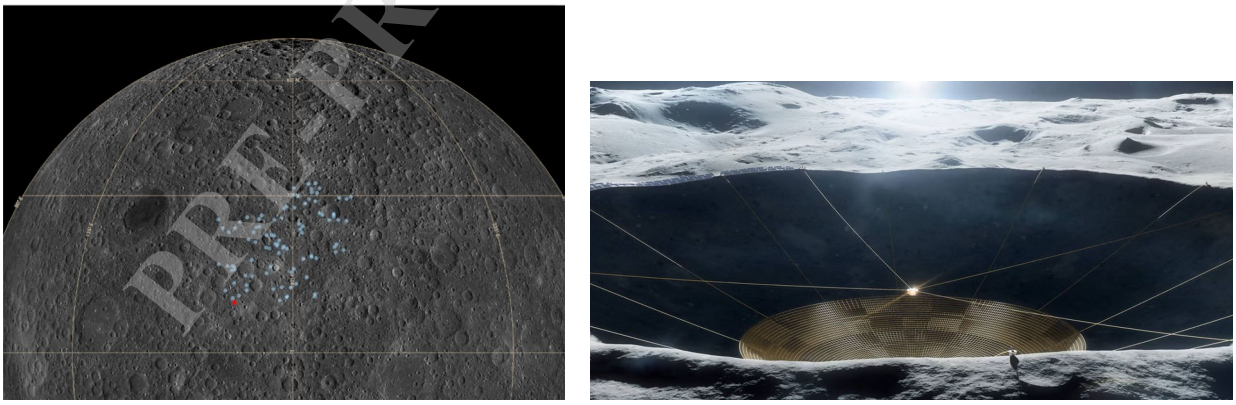

a) b)

Fig. 23. a) There are over 82,000 craters on the far side of the Moon, ranging in size from 3 to 5 km in diameter. The 50 candidates suitable for a 1,000 m diameter antenna are marked in blue, while the crater selected for NASA concept is marked in red [19]. *b) NASA concept to place a 1,000-meter radio telescope on the far side of the Moon* [23], [24]

Caustics formed by gravitational lenses are an important element in deep space research. Two forms of such caustics can be distinguished. The first is the case when a distant object, a massive structure obscuring it and creating a gravitational lens, and the observer are located on one line. This gives the chance to assess the distance to the object by spectral analysis of the light condensed on a caustic (Fig. 24a).

In the second case, these objects are not located axially and a caustic has a complex form or consists of many elements. Then, the possibility arises that individual elements of the caustics guide light that has traveled a different distance. This provides information about a distant object at different stages of its evolution (Fig. 24b).

a) b)

Fig. 24.The gravity of the bright massive object in the foreground bends the light of an unseen distant galaxy. A light oval is a cross-section of the caustics seen from the front. a) A distant invisible object, a structure forming a gravitational lens and an observer are in a straight line [26]. *b) These objects are not located axially and a caustic has a complex form or consist of many elements* [27].

8. CONCLUDING REMARKS

In many leading fields of science, it can be pointed out that the solutions used today were known much earlier, often being used in very distant applications. The article shows how the concept of focusing light by a concave mirror, discovered by Leonardo da Vinci about 500 years ago, is developing in contemporary fields of science and technology.

Leonardo showed that only about 0.4% of the surface of a hemispherical mirror is needed to concentrate the energy of solar rays, while the rest of the bowl remains useless [13]. This

observation is entirely valid. Developments in this field of observation show that the diameter of the mirrors of both historical and modern optical telescopes, as well as radio telescopes, constitutes only a small fraction of the hemisphere. As a result of the development of receiving techniques, the mirror aperture used to create the focusing effect has increased significantly. The implementation of this progress are the radio telescopes in Arecibo (Puerto Rico) and Dawodang (China) with a bowl diameter of 300 m and 500 m, respectively. The presence of Leonardo's concepts in such distant areas as the reception of light or radio waves coming from deep space and studies on future deployment large-scale observation devices on the Moon is also spectacular [24, 28].

During the research on the formation of the mirror focus, Leonardo showed that there was an area around the focus where reflected rays also concentrate. This effect is known today as caustics and its presence is used in many fields of technology and science. The caustics he graphically constructed also arise in the acoustic field in rooms. However, the response of a room to broadband sound stimulation, i.e., music or speech, makes it difficult to identify caustics audibly. As a result, the effect of sound concentration by arched vaults and concave walls of rooms takes the form of a blurred area with an increased sound level and unusual values of acoustic parameters. For this reason, the concept of caustics is almost absent in the field of architectural acoustics. The literature on the subject clearly indicates that large, concave interior surfaces in rooms are acoustically unfavorable, even though they are commonly employed in architectural design. As the article notes, in many practical circumstances, this unfavorable effect partially or completely disappears and becomes less harmful.

This paper presents an analytical description of caustics for an infinitely distant ray source and a source located at a given distance from the mirror. Interference occurring on a caustic when light rays incident on the mirror are treated as waves are also investigated. This phenomenon is discussed for acoustic and electromagnetic waves. In addition to the applications presented, caustics are found in numerous fields of technology and science, e.g., in laser technology, underwater exploration, crystallography, metallurgy, and many other fields.

APPENDIX

Reduction of Eq. (3.4), (3.5) to the form (2.3) when d→∞

$$\begin{cases} x(\theta) = R\left(-\cos(\theta) + \sin(\theta)\times \mathrm{tg}\left(\Gamma(\theta)\right)\right)\times \cos^2\left(\Gamma(\theta)\right)\times \boxed{\dfrac{R^2 + d^2 + 2Rd\sin(\theta)}{R^2 + 2d^2 + 3Rd\sin(\theta)}} + R\cos(\theta) & (3.4) \\ y(x,\theta) = \left(x(\theta) - R\cos(\theta)\right)\mathrm{tg}\left(\Gamma(\theta)\right) - R\sin(\theta) & (3.5) \end{cases}$$

where $\Gamma(\theta) = \arcsin\left(\boxed{\dfrac{d\cos(\theta)}{\sqrt{R^2 + d^2 + 2Rd\sin(\theta)}}}\right) - \theta$, $0 \le \theta \le \Pi$

For d→∞ the terms containing d (see boxes) tend to cos(*θ*) and 1/2:

$$\lim_{d\to\infty}\left(\frac{d\cos(\theta)}{\sqrt{R^2 + d^2 + 2Rd\sin(\theta)}}\right) = \lim_{d\to\infty}\left(\frac{d\cos(\theta)}{d\sqrt{\frac{R^2}{d^2} + \frac{d^2}{d^2} + \frac{2Rd\sin(\theta)}{d^2}}}\right) = \frac{\cos(\theta)}{\sqrt{0+1+0}} = \cos(\theta)$$

$$\lim_{d\to\infty}\left(\frac{R^2 + d^2 + 2Rd\sin(\theta)}{R^2 + 2d^2 + 3Rd\sin(\theta)}\right) = \lim_{d\to\infty}\left(\frac{d^2\left(\frac{R^2}{d^2} + \frac{d^2}{d^2} + \frac{2Rd\sin(\theta)}{d^2}\right)}{d^2\left(\frac{R^2}{d^2} + \frac{2d^2}{d^2} + \frac{3Rd\sin(\theta)}{d^2}\right)}\right) = \frac{0+1+0}{0+2+0} = \frac{1}{2}$$

After substituting these values into Eq. (3.4), (3.5), they take the form (2.3) [10].

$$\begin{cases} x(\theta) = R\cos^3(\theta) \\ y(\theta) = \dfrac{R}{2}\left(2\sin^3(\theta) - 3\sin(\theta)\right) \end{cases} \qquad 0 \le \theta \le \Pi \qquad (2.3)$$

DECLARATION OF CONFLICTING INTERESTS

The author declares that there are no known competing financial interests or personal relationships that could have influenced the work reported in this paper.

REFERENCES

[1] https://in.pinterest.com/pin/667306869763527291/ (access: 06.06.2025)

[2] https://in.pinterest.com/pin/321866704609051258/ (access: 06.06.2025)

[3] Jankowski L J. Wyznaczanie współczynnika intensywności naprężeń metodami optycznymi – materiały pomocnicze (Determination of the stress intensity factor by optical methods, in Polish); 2011. < http://www.biomech.pwr.wroc.pl/wpcontent/uploads/ 2016/ 09/pdcw14.pdf > (access: 06.06.2025).

[4] https://atoptics.co.uk/blog/reflection-caustics/ (access: 06.06.2025)
[5] https://www.pxfuel.com/en/search?q=strommast (access: 06.06.2025)
[6] https://old.atoptics.co.uk/fz552.htm (access: 06.06.2025)
[7] https://commons.wikimedia.org/wiki/Category:Caustics_(optics)?uselang=en (access: 04.10.2025)
[8] Castagnede B, et al. Cuspidal caustic and focusing of acoustical waves generated by a parametric array onto a concave reflecting surface. C. R. Mecanique, 337; 2009. DOI: 10.1016/j.crme.2009.09.006 > [access: 03.10.2025]
[9] Kulowski A., The caustic in the acoustics of historic interiors. *Applied Acoustics* 133 (2018) 82–90, https://doi.org/10.1016/j.apacoust.2017.12.008 (access: 06.06.2025)
[10] Kulowski A., Analysis of a caustic formed by a spherical reflector: Impact of a caustic on architectural acoustics, *Applied Acoustics* 165 (2020), https://doi.org/10.1016/j.apacoust.2020.107333 (access: 06.06.2025)
[11] http://hyperphysics.phy-astr.gsu.edu/hbase/phyopt/Raylei.html (access: 03.09.2025)
[12] Burkhard D.G., Shealy D.L., Formula for the density of tangent rays over a caustic surface. *Applied Optics* vol. 21, No. 18, 3299–06 (1982).
[13] Kulowski A., Do Leonardo da Vinci's drawings, room acoustics and radio astronomy have anything in common? *Heritage Science (2022) 10:104,* https://doi.org/10.1186/s40494-022-00713-6 (access: 06.06.2025)
[14] Barron M., *Auditorium acoustics and architectural design*. E&FN Spon, London - New York (1998)
[15] http://poznanfilmcommission.pl/lokacja/aula-uam. (access: 06.06.2025)
[16] Kamisiński T., Pilch A., Rubacha J. Large format acoustic structures in the concert halls. *EuroRegio 2016; Spanish Congress on Acoustics TECNIACUSTICA 2016,* Porto, Portugal
[17] Kamisiński T., Zagadnienia akustyki zabytkowych sal teatralnych na planie podkowy (Acoustic Issues in Historic Horseshoe-Planned Theatre Halls. In Polish). *Rozprawy Monografie* nr 255, Wydawnictwa AGH, Kraków 2012
[18]https://tereska12045.flog.pl/ archiwum/ albumy/ 232073/trojmiasto/[06.06.2025]
[19] https://dbt.arch.ethz.ch/project/acoustic-mirrors/ (access: 06.06.2025)
[20] https://www.space.com/38217-arecibo-observatory-puerto-rico-telescope-photos.html (access: 06.06.2025)
[21] https://www.youtube.com/watch?v=3oBCtTv6yOw (access: 06.06.2025)
[22] https://www.youtube.com/watch?v=dPWmdcAKSFA (access: 06.06.2025)
[23] https://www.nasa.gov/directorates/spacetech/niac/2020_Phase_I_Phase_II/ lunar_crater_radio_telescope/ (access: 06.06.2025)
[24] S. Bandyopadhyay et al. Conceptual Design of the Lunar Crater Radio Telescope (LCRT) on the Far Side of the Moon. *2021 IEEE Aerospace Conference*, March 2021. DOI: 10.1109/AERO50100.2021.9438165 (access: 06.06.2025)
[25] https://phys.org/news/2023-09-big-observatories-built-moon.html (access: 06.06.2025)
[26] https://www.euclid-ec.org/einstein-ring-in-ngc-6505/ (access: 06.06.2025)
[27] https://en.wikipedia.org/wiki/Gravitational_lens (access: 06.06.2025)
[28] Skowron J., Analiza niestandardowych zjawisk mikrosoczewkowania grawitacyjnego gwiazd Galaktyki. Rozprawa doktorska (Analysis of non-standard phenomena of gravitational microlensing of Galactic stars. PhD dissertation, in Polish). Uniwersytet Warszawski (2009) http://www.astrouw.edu.pl/~jskowron/PhD/thesis/phd.pdf (access: 06.06.2025)